ce/papers Proceedings in civil engineering

Ernst & Sohn A Wiley Brand

Check for updates

Full paper

Seismic Performance Assessment of CFS Strap-Braced Walls Using Optimised Sections

Muhammed Cosut[1] | Seyed Mohammad Mojtabaei[2] | Sarmad Shakeel[1] | Iman Hajirasouliha[1]

Correspondence

PhD Candidate, Muhammed Cosut
University of Sheffield
School of Mechanical, Aerospace and Civil Engineering
Mappin Street
S1 3JD Sheffield
Email: mcosut1@sheffield.ac.uk

[1] Department of Civil and Structural Engineering, The University of Sheffield, Sheffield, UK
[2] School of Architecture, Building and Civil Engineering, Loughborough University, Leicestershire, UK

Abstract

Light steel-framed buildings using cold-formed steel (CFS) profiles are common in low- to mid-rise structures, with CFS strap-braced frames as primary lateral force-resisting systems. This study investigates CFS strap-braced walls, in which the studs are optimised as beam-column elements, to improve seismic performance and design efficiency. A representative cross-section, based on commercially available profiles, is selected and optimised to achieve maximum load-bearing capacity while complying with standard and market constraints. Finite element (FE) models of CFS strap-braced walls with both commercially available and optimised stud sections are then developed. The influence of gravity loads, which is ignored in the conventional design of CFS strap-braced walls, is examined by applying various load intensities based on the total compressive strength of the chords and studs. Performance evaluation involves the compliance against maximum allowable drift limits without any premature failure due to the P-Δ effect in the chord studs. The findings contribute to the advancement of seismic design methodologies for CFS structures by providing a framework for optimising CFS strap-braced frames, thereby enhancing their ductility, safety, and stability in earthquake-prone regions.

Keywords

Cold-Formed Steel, Strap-Braced Wall, Optimization, Gravity Loading, Seismic Performance.

1 Introduction

Cold-formed steel (CFS) offers significant advantages, including a high strength-to-weight ratio, durability, and recyclability, making it a sustainable and cost-effective choice. Its lightweight nature facilitates transportation and quick installation, while its adaptability allows for efficient section design and off-site manufacturing, reducing waste and construction time. Additionally, CFS members can serve as primary force-resisting systems in multi-storey structures, effectively withstanding both vertical and lateral forces from wind and earthquakes. In these structures, strap-braced stud walls provide lateral load resistance, with bracing systems available in various configurations such as X-shaped [1], K-braced [2], knee-braced, or combinations of these types.

Various studies [1-3] have explored the behaviour of CFS strap-braced walls, particularly their performance under monotonic and cyclic loading. Al-Kharat and Rogers [1] conducted experimental evaluations of light, medium, and heavy CFS strap-braced walls, revealing that heavy panels exhibited insufficient ductility. Similarly, Zeynalin and Ronagh [3] investigated CFS strap-braced walls with a 1:1 aspect ratio, analysing the influence of strap quantities, angles and brackets under cyclic loading. Their findings demonstrated that these walls exhibited stable hysteretic performance and could be considered structurally reliable. While shake-table test performed by [4] have provided insights into CFS wall behaviour, the combined effects of gravity and lateral loads have often been overlooked. Rad et al. [5] addressed this limitation by conducting full-scale cyclic tests on two-story CFS strap-braced systems, demonstrating a strong elastic-plastic response when proper detailing was applied.

Optimization techniques are widely used in structural engineering to maximise capacity and stiffness or to minimise cost, carbon emission and weight. Various algorithms, including metaheuristic, deterministic (gradient-based), and hybrid approaches, can be employed depending on the design objectives. Ye et al. [6] increased beam

© 2026 The Author(s). Published by Ernst & Sohn GmbH.

https://doi.org/10.1002/cepa.70206 wileyonlinelibrary.com/journal/cepa

This is an open access article under the terms of the Creative Commons Attribution License, which permits use, distribution and reproduction in any medium, provided the original work is properly cited.

load-carrying capacity by optimizing various cross-sectional configurations, incorporating edge and intermediate stiffeners along with segmentally folded flanges. Similarly, Mojtabaei et al. [7] developed an optimal design methodology for CFS beam-column members using a metaheuristic algorithm to maximise load-carrying capacity while maintaining constant material use, following Eurocode 3.

This study aims to maximise the load-bearing capacity of CFS strap-braced walls by replacing the commercially available stud section used in them by the optimised counterparts. The optimisation process was constrained by the material usage (total coil width and thickness) of the selected section. FE models of walls with both the commercially available and optimised stud sections were developed and analysed under gravity and lateral loads to assess their seismic performance. Following this introduction, Section 2 presents the design process of the CFS beam-column elements, while Section 3 outlines the optimisation method and associated constraints. Section 4 describes the development and verification of the FE model, and Section 5 evaluates the seismic performance.

2 CFS beam-column element design according to Eurocode

In this study, the capacity of the CFS beam-column element was determined using the EN1993-1-1 [8], EN1993-1-3 [9] and EN1993-1-5 [10] standards. The cross-sectional resistance was evaluated by considering both local and distortional buckling modes, while the member resistance accounted for global instabilities.

2.1 Local-distortional buckling and cross-section check

The Effective Width Method (EWM) in Eurocode 3 accounts for local buckling by reducing the load-carrying capacity in compressed plate areas, potentially shifting the centroid and introducing additional bending moments. Under bending, an iterative process is used to locate the neutral axis and calculate the bending strength using the effective partially plastic section modulus. Distortional buckling, which commonly occurs in stiffened plates subjected to flexural or flexural-torsional loading, involves a combination of in-plane and out-of-plane deformations. Eurocode 3 addresses this by reducing the effective thickness of the stiffener and adjacent plate regions, with buckling stress calculated by modelling the stiffened section as a compression element on an elastic foundation.

The cross-section of a CFS beam-column under axial compression and bending moments must satisfy the following criteria:

$$\frac{N_{Ed}}{N_{c,Rd}} + \frac{M_{y,Ed} + \Delta M_{y,Ed}}{M_{cy,Rd}} + \frac{M_{z,Ed} + \Delta M_{z,Ed}}{M_{cz,Rd}} \leq 1 \quad (1)$$

where $N_{c,Rd}$ denotes the design compressive resistance of the cross-section, while $M_{cy,Rd}$ and $M_{cz,Rd}$ design moment resistance about the major (y-axis) and the minor (z-axis) axes, respectively. The additional moments are calculated as $\Delta M_{y,Ed} = N_{Ed} e_{Ny}$ and $\Delta M_{z,Ed} = N_{Ed} e_{Nz}$, where e_{Ny} and e_{Nz} are the shifts of the y- and z-axes, respectively.

2.2 Member resistance

Member resistance requires various calculations for both pure compression and pure bending. In this regard, global buckling is considered for pure compression, while lateral-torsional buckling is assessed under pure bending. Additionally, member stability was evaluated using the equations provided in EN 1993-1-3.

3 Optimization process

The optimisation process in this study was performed using the optimisation code developed by Mojtabaei et al. [7], which employs the Particle Swarm Optimization (PSO) algorithm. The objective was to maintain the same material usage (i.e., total coil width) as the commercially available reference section, which served as the benchmark. Based on this reference, an optimised cross-section was generated to enhance the load-bearing capacity under axial compression (N_{Ed}) and major axis bending moment ($M_{y,Ed}$). The bending moment was introduced through an eccentric (e_y) axial compressive load to effectively maximise the axial capacity N_{Ed} under realistic loading conditions.

$$M_{y,Ed} = N_{Ed} \times e_y \quad (2)$$

In the optimization process, a simply supported beam-column element with end-fork supports was used, allowing rotations and warping at the ends, while preventing twisting along the member's longitudinal axis. This study adopts a lipped channel section and examines various parameters, including section thicknesses (1.16, 2, 3, and 4 mm) and eccentricities (0, 100, and 300 mm), to evaluate and compare the axial compressive load capacity improvements across different cases. To achieve the maximum axial load-bearing capacity, the Eurocode Design Procedure for Beam-Column Members and PSO optimization tool in MATLAB were applied for cross-sectional optimization.

The initial and optimised cross-sectional shapes are demonstrated in Figure 1. In addition, specific limitations and constraints defined by standards and the manufacturing process, are provided in Table 1. The design variables were based on the flange and lip lengths, which are constrained by these standards and the manufacturing process. The value of θ was taken as $\pi/2$. Additional constraints were applied to ensure proper installation of the hold-downs (Simpson S/HD10 S, 59 mm depth) on the CFS strap-braced wall. This constraint focused on the spacing between the lips of the chord members, ensuring adequate clearance for the hold-downs to fit securely without interfering with the cross-sectional geometry of the chords, as follows:

$$spacing \geq h - 2 \times c = 60 \quad (3)$$

where *h* denotes the web height and *c* represents the lip length.

Table 1 Optimization design variables, constraints and limitations

Design Variables	Constraints based on EC3	Manufacturing & practical limitations (mm)
$\boldsymbol{X_1 = c/b}$ $\boldsymbol{X_2 = b/L}$	$0.2 \leq c/b \leq 0.6$ $b/t \leq 60$ $c/t \leq 50$ $h/t \leq 500$ $\pi/4 \leq \theta \leq 3\pi/4$	$b \geq 30$ $c \geq 10$ $h \geq 2csin(\theta)$

25097075, 2025, 6, Downloaded from https://onlinelibrary.wiley.com/doi/10.1002/cepa.70206 by Open Access Sheffield - UNIVERSITY OF SHEFFIELD , Wiley Online Library on [29/01/2026]. See the Terms and Conditions (https://onlinelibrary.wiley.com/terms-and-conditions) on Wiley Online Library for rules of use; OA articles are governed by the applicable Creative Commons License

Design variables which are X_1 and X_2 ratio ranges were computed based on the standard and manufacturing process. X_1 was set between 0.2 and 0.6, while X_2 was determined based on the total coil width and material thickness. The maximum ratio for X_2 was limited using two different arrangements to reduce the computational time by narrowing the range.

$$\frac{b_{min}}{L} \leq X_2 \leq \min \begin{cases} \frac{60 \times t}{L} \\ \frac{b_{msx}}{L} \end{cases} \quad (4)$$

$$b_{msx} = L - h_{min} - 2 \times c_{min} \quad (5)$$

where b_{min} was set 30 mm, L is the total coil width (300 mm), t, h_{min}, c_{min} represent the thickness, minimum web height and minimum lip length, respectively.

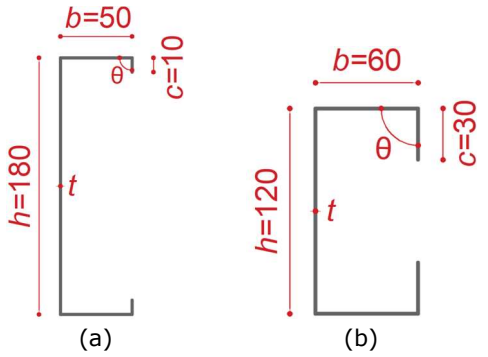

Figure 1 Cross section of: (a) commercially available, (b) optimised section

3.1 Particle Swarm Optimization (PSO)

Particle Swarm Optimization (PSO), introduced by Kennedy and Eberhart [11], is a metaheuristic algorithm inspired by the collective behaviour of social organisms such as ants, fish, and birds. Drawing from these natural swarm dynamics, PSO falls within the broader category of swarm intelligence techniques. Its fundamental mechanism allows particles to adaptively update their velocities based on both their own previous best performance and that of the entire swarm, resulting in an effective combination of individual learning and group coordination.

4 FE modelling: descriptions and properties

Abaqus [12] has been widely recognised for its capability in accurately simulate the structural behaviour of CFS wall panels, minimising the need for extensive experimental testing. Following the optimization of the C-lipped section with zero eccentricity (e= 0), FE models of CFS strap-braced walls were developed using both commercially available and optimised stud sections. Each wall model measured 2.44 m × 2.44 m and included top and bottom rigid plates, tracks, chords, studs, X-shaped straps, bridging members, hold-downs, L-brackets, and anchor rods (see in Figure 2).

4.1 Element type and material characterization

The CFS strap-braced walls were modelled using four-noded S4R shell elements, which are suitable for thin-walled structures. A mesh sensitivity analysis led to a 15 mm × 15 mm mesh for most members, with a 20 mm × 20 mm mesh for thick plates to reduce computational demand.

Material properties were obtained from experimental tests, and stress-strain data was converted to true stress-strain relationships for accurate Abaqus input. The elastic modulus is 203 GPa, and the Poisson's ratio is 0.3. Strap and track have the same yield (f_y) and ultimate stress (f_u) as 296 and 366 MPa, respectively. Also, stud and chord have the same f_y and f_u of 325 and 382 MPa, respectively. In addition, the isotropic hardening model was used for the monotonic analysis.

Table 2 Material properties

	f_y (MPa)	f_u (MPa)
Strap Track	296	366
Stud Chord	325	382

4.2 Boundary conditions, loading and connection modelling

In the FE model, hold-downs (Simpson S/HD10 S) and tracks were coupled to reference points aligned with the anchor locations. The bottom reference points were fully constrained, while the top reference points allowed in-plane lateral displacement, with out-of-plane translational and rotational movements restrained. Monotonic loading was applied up to a maximum allowable inter-storey drift of 5% [13]. To simulate gravity effects, a 20 mm thick plate was placed above the top track to ensure uniform load distribution. The top plate was subjected to a uniform pressure, proportional to the compressive strength of the vertical elements, as specified by EN1993-1-3 [9].

The track-to-stud and strap-to-chord screw connections were modelled using Pham and Moen's empirical equations [14]. In Abaqus [12], screws were represented as discrete fasteners, with each connector's influence radius linking surface node displacements and rotations to fastening points.

4.3 Geometric imperfection

Initial geometric imperfections were incorporated by scaling the first buckling mode shape from an eigenvalue buckling analysis, following Schafer and Peköz [15]. Slack in tension straps was simulated by applying unit lateral displacements at anchor points, inducing initial compression in the diagonals. Chord stud imperfections were omitted due to their negligible impact [16], enhancing computational efficiency in multi-storey models.

25097075, 2025, 6, Downloaded from https://onlinelibrary.wiley.com/doi/10.1002/cepa.70206 by Open Access Sheffield - UNIVERSITY OF SHEFFIELD , Wiley Online Library on [29/01/2026]. See the Terms and Conditions (https://onlinelibrary.wiley.com/terms-and-conditions) on Wiley Online Library for rules of use; OA articles are governed by the applicable Creative Commons License

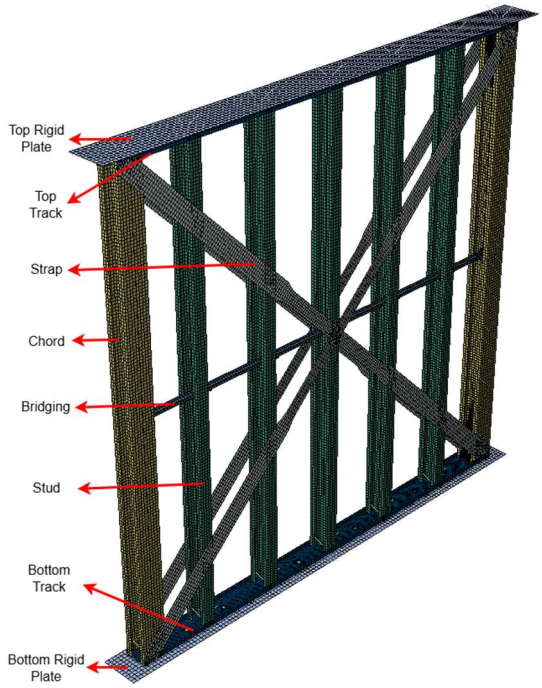

Figure 2 FE model

5 Results

In the optimization process, three different values of e (0, 100, and 300) were considered, along with four thicknesses (1.16, 2, 3, and 4) for the C-lipped stud element. These combinations were analysed to explore the relationship between e and thickness. The results show that as e increases, the capacity improvements between commercially available and optimised sections become smaller. To exemplify, the capacity improvement for e=0 ranges from approximately 42% to 91%, while for e=300, it ranges from about 8% to 25% (see Figure 3). Consequently, the differences in average capacity improvement of approximately 45% and 12% can be observed between e=0 and e=300, as well as between e=100 and e=300, respectively.

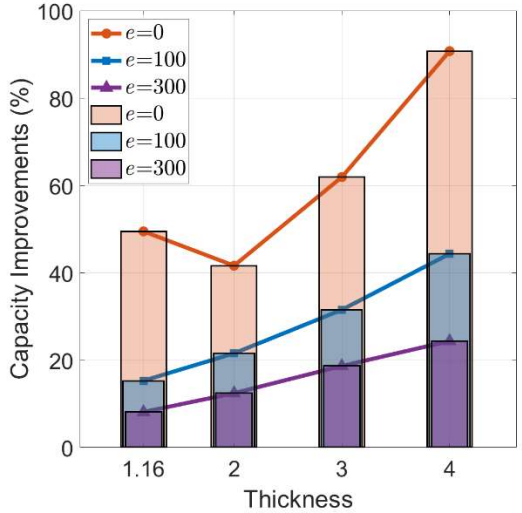

Figure 3 Optimization results based on thickness and *e*

Once the CFS strap-braced wall frames using both commercially available and optimised stud sections were created in Abaqus, the gravity load, calculated based on commercially available section considering the total compressive strength of the vertical elements ($N_{b,t}$), was applied to both frames across a range of load levels. This was done to examine the P- Δ responses of the models and to assess whether they reached the maximum allowable drift.

Figure 4 illustrates the FE analysis results, showing the effects of applying gravity loads ranging from 0% to 50% $N_{b,t}$ on both frames. The analysis was conducted using 2 mm thick straps and 1.16 mm thick chords and studs. The CFS strap-braced frame equipped with the optimised section (see Figure 4 (b)) demonstrated consistent performance, with most frames achieving the maximum allowable drift. However, the frames subjected to 43% and 50% $N_{b,t}$ are unable to reach this limit. In contrast, CFS strap-braced frame equipped with commercially available stud section (see Figure 4 (a)) showed a noticeable reduction in performance, failing to reach the maximum allowable drift at several load levels between 22% and 50% $N_{b,t}$.

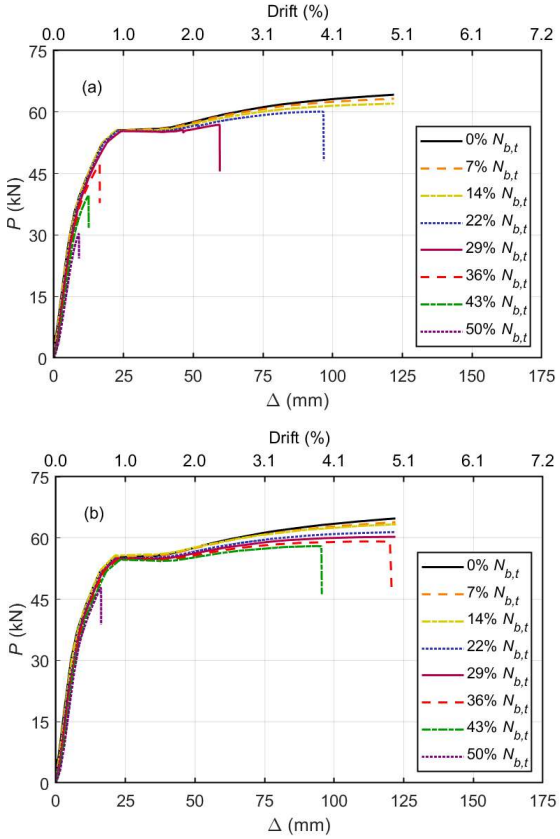

Figure 4 Monotonic response of (a):commercially available; (b): optimised models

The stiffness (k) (kN/mm) and ductility (μ) values were computed using the bilinear curve shown in Figure 5, which follows the Equivalent Energy Elastic-Plastic (EEEP) approach [17]. These values are determined as follows:

$$k = \frac{P_y}{\Delta_y} \tag{6}$$

$$\mu = \frac{\Delta_u}{\Delta_y} \tag{7}$$

where P_y is the yield load, Δ_y is the yield displacement, and Δ_u is the ultimate displacement.

25097075, 2025, 6, Downloaded from https://onlinelibrary.wiley.com/doi/10.1002/cepa.70206 by Open Access Sheffield - UNIVERSITY OF SHEFFIELD , Wiley Online Library on [29/01/2026]. See the Terms and Conditions (https://onlinelibrary.wiley.com/terms-and-conditions) on Wiley Online Library for rules of use; OA articles are governed by the applicable Creative Commons License

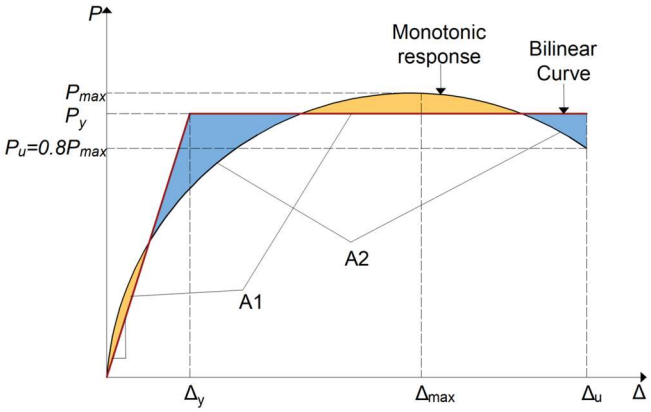

Figure 5 Bilinear curve based on monotonic response

Based on monotonic analysis results, the stiffness and ductility of both CFS strap-braced frames, equipped with commercially available and optimised stud sections, were evaluated under varying vertical load ratios (% $N_{b,t}$) (see Figure 6). The stiffness of both models exhibits a similar decreasing trend, with a gradual reduction as the vertical load increases. For frames with commercially available stud section, ductility shows a slight decline from 0% to 14% $N_{b,t}$, followed by a significant drop beyond this point. In contrast, frames with optimised stud section maintains higher ductility up to 36% $N_{b,t}$, with a noticeable reduction occurring only at higher vertical load levels. A sharp drop is observed particularly at 50% $N_{b,t}$, where the ductility value reaches approximately 1.4.

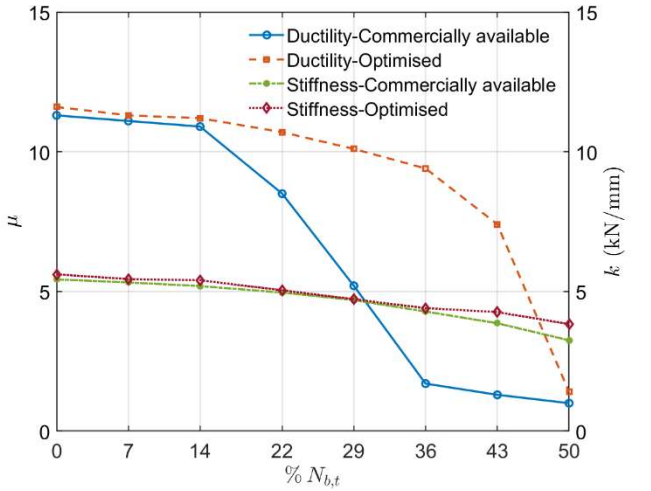

Figure 6 Evaluation of ductility ratio *(μ)* and stiffness *(k)* of the commercially available and optimised section under varying $N_{b,t}$

6 Conclusion

This study aimed to enhance the performance of CFS strap-braced frames by optimising stud (beam–column) sections within design and manufacturing constraints. The optimised cross-section was applied to both studs and chords, and FE models were developed in Abaqus using both commercially available and optimised stud sections. Combined gravity and lateral loads were applied to the frames, with the total gravity load calculated based on the compressive strength of the vertical elements (i.e., chords and studs) in the commercially available section. This reference value was then used to define gravity load levels ranging from 0% to 50% of $N_{b,t}$, and consistently applied to both frames. This approach enabled a consistent comparison of stiffness, strength, and ductility across configurations.

- The findings demonstrate that variations in eccentricity (e) and thickness during beam–column element optimization significantly influence to the improvement of the load-bearing capacity, revealing clear differences between the optimised and commercially available sections. Moreover, increased eccentricity results in reduced capacity.
- While low vertical loads have a minimal impact on lateral performance, higher gravity loads considerably enhance the peak strength, ductility, and stiffness of frames incorporating the optimised section, in contrast to those using commercially available section.

References

[1] Al-Kharat, M.; Rogers, C.A. (2007) *Inelastic performance of cold-formed steel strap braced walls.* Journal of Constructional Steel Research 63, 4, p. 460–474.

[2] Riahi, H.T. et al. (2020) *Seismic collapse assessment of K-shaped bracings in cold-formed steel frames.* Structures 27, p. 1803–1817.

[3] Zeynalian, M.; Ronagh, H. (2013) *Experimental study on seismic performance of strap-braced cold-formed steel shear walls.* Advances in Structural Engineering 16, 2, p. 245–257.

[4] Gad, E. et al. (1999) *Lateral performance of cold-formed steel-framed domestic structures.* Engineering Structures 21, 1, p. 83–95.

[5] Rad, P.L. et al. (2024) *Experimental investigation on seismic performance of cold-formed steel strap-braced stud walls under lateral cyclic and vertical loading.* Thin-Walled Structures 194, p. 111312.

[6] Ye, J. et al. (2016) *Development of more efficient cold-formed steel channel sections in bending.* Thin-Walled Structures 101, p. 1–13.

[7] Mojtabaei, S.M. et al. (2021) *Structural size optimization of single and built-up cold-formed steel beam-column members.* Journal of Structural Engineering 147, 4, p. 04021030.

[8] CEN (European Committee for Standardization) (2005) *Eurocode 3: Design of steel structures – Part 1-1: General rules and rules for buildings.* Brussels, Belgium.

[9] CEN (European Committee for Standardization) (2005) *Eurocode 3: Design of steel structures – Part 1-3: General rules – Supplementary rules for cold-formed members and sheeting.* Brussels, Belgium.

[10] CEN (European Committee for Standardization) (2006) *Eurocode 3: Design of steel structures – Part 1-5: Plated structural elements.* Brussels, Belgium.

[11] Kennedy, J.; Eberhart, R. (1995) *Particle swarm optimization*. Proceedings of ICNN'95 – International

25097075, 2025, 6, Downloaded from https://onlinelibrary.wiley.com/doi/10.1002/cepa.70206 by Open Access Sheffield - UNIVERSITY OF SHEFFIELD , Wiley Online Library on [29/01/2026]. See the Terms and Conditions (https://onlinelibrary.wiley.com/terms-and-conditions) on Wiley Online Library for rules of use; OA articles are governed by the applicable Creative Commons License

Conference on Neural Networks, pp. 1942–1948.

[12] Dassault Systèmes Simulia (2014) *Abaqus 6.14 CAE User Guide.*

[13] Building Seismic Safety Council (2000) *Prestandard and commentary for the seismic rehabilitation of buildings*. FEMA-356 Report, Washington, DC.

[14] Pham, H.S.; Moen, C.D. (2015) *Stiffness and strength of single shear cold-formed steel screw-fastened connections.* Proceedings of the Annual Stability Conference, p. 1–12.

[15] Schafer, B.W.; Peköz, T. (1998) *Computational modeling of cold-formed steel – Characterizing geometric imperfections and residual stresses.* Journal of Constructional Steel Research 47, 3, p. 193–210.

[16] Papargyriou, I. et al. (2021) *Performance-based assessment of CFS strap-braced stud walls under seismic loading.* Journal of Constructional Steel Research 183, p. 106731.

[17] AISI (American Iron and Steel Institute) (2007) *North American standard for cold-formed steel framing – Lateral design. AISI S213-07*, Washington, DC.

25097075, 2025, 6, Downloaded from https://onlinelibrary.wiley.com/doi/10.1002/cepa.70206 by Open Access Sheffield - UNIVERSITY OF SHEFFIELD , Wiley Online Library on [29/01/2026]. See the Terms and Conditions (https://onlinelibrary.wiley.com/terms-and-conditions) on Wiley Online Library for rules of use; OA articles are governed by the applicable Creative Commons License